Long-Lived, High-Strength States of ICAM-1 Bonds to β_2 Integrin, II: Lifetimes of LFA-1 Bonds Under Force in Leukocyte Signaling

Koji Kinoshita,[†‡] Andrew Leung,[‡] Scott Simon,[§] and Evan Evans[†‡*]
[†]Department of Biomedical Engineering, Boston University, Boston, Massachusetts; [‡]Department of Physics and Pathology, University of British Columbia, Vancouver, Canada; and [§]Department of Biomedical Engineering, University of California, Davis, California

ABSTRACT Using single-molecule force spectroscopy to probe ICAM-1 interactions with recombinant α_L β_2 immobilized on microspheres and β_2 integrin on neutrophils, we quantified an impressive hierarchy of long-lived, high-strength states of the integrin bond, which start from basal levels with activation in solutions of divalent cations and shift dramatically upward to hyper-activated states with cell signaling. Taking advantage of very rare events, we used repeated measurements of bond lifetimes under steady ramps of force to achieve a direct assay for the off-rates of ICAM-1 from β_2 integrin throughout the course of each experiment. In our companion article I, we demonstrate the assay using results from tests of a monovalent ICAM-1 probe against recombinant α_L β_2 on microspheres in millimolar solutions of divalent cations (Ca^{2+}, Mg^{2+}, Mn^{2+}). In this article, we examine the impact of inside-out and outside-in signaling in neutrophils on the lifetimes and mechanical strengths of ICAM-1 bonds to β_2 integrin on the cell surface. Even though ICAM-1 bonds to recombinant α_L β_2 on microspheres in Mg^{2+} or Mn^{2+} can live for long periods of time under slow pulling, here we show that stimulation of neutrophils in Mg^{2+} plus the chemokine IL-8 (i.e., inside-out signaling) induces several-hundred-fold longer lifetimes for ICAM-1 attachments to LFA-1, creating strong bonds at very slow pulling speeds where none are perceived in Mg^{2+} or Mn^{2+} alone. Similar changes are observed with outside-in signaling, i.e., long lifetimes and increased bond strength also occur when neutrophils are bound with the activating (anti-CD18) monoclonal 240Q. Limiting our investigation to rare events using very dilute ICAM-1 probes, we show that although the prolonged lifetimes of cell surface attachments for both inside-out and outside-in signaling exhibit single-bond-like statistics for dissociation under force, they are consistent with a tightly coupled dimeric ICAM-1 interaction with a pair of LFA-1 heterodimers.

INTRODUCTION

Circulating leukocytes selectively adhere to and migrate through the vascular endothelium proximal to sites of tissue injury or infection. Mediating this recruitment process are multiple sets of adhesion molecules (1) that appear or disappear, or become active or inactive, through regulation by signaling molecules either endogenous to the vascular cells (cytokines) or arising from other pathogenic sources (chemokines). The subset of interactions involving β_2 integrins plays a prominent role in the firm adhesion of leukocytes, which enables cell spreading and emigration into tissues (2). Like all integrins, the large heterodimers exhibit geometries in electron micrographs that range from bent or collapsed shapes correlating with imperceptible adhesion to extended or erect shapes correlating with different levels of adhesiveness (3,4,5,6). It is well known (2–7) that integrins change their conformations and levels of adhesiveness in vivo through processes known as outside-in and inside-out signaling, which involve cellular chemical pathways initiated in the first case by ligand binding and in the second by chemokine or cytokine stimulation.

Integrin adhesiveness, or avidity (7), is believed to involve both the density and arrangements of integrin sites for binding multiple ligands along with the chemical affinity for binding ligand. Different arrangements of integrins have been correlated with different types of cell adhesion (8,9,10); however, in experiments combining fluorescence resonance energy transfer (FRET) with high-resolution fluorescence imaging, Kim et al. (11) refined the phenomenology of arrangements by distinguishing between microclusters on a scale of ~1 nm and macroclusters on a scale of $\geq$200 nm. As emphasized in the title of their work (11), they concluded that the experiments showed a ''primacy of affinity over clustering in regulation of adhesiveness'' of lymphocyte function-associated antigen-1 (LFA-1) when bound by intercellular adhesion molecule-1 (ICAM-1). Of particular relevance to the study presented here, binding monomeric ICAM-1 to leukocytic cells in Mn^{2+} appeared to induce neither micro- nor macroclustering of LFA-1. On the other hand, binding dimeric ICAM-1fc resulted in efficient microclustering but no macroclustering. Moreover, binding diICAM-1 to cells stimulated by chemokine induced robust microclustering of LFA-1, again with no detectable macroclustering. Consistent with these observations, we find that specific attachments readily form between a force probe linked with dilute diICAM-1 and neutrophils in millimolar solutions of Mn^{2+} or solutions of Mg^{2+} plus chemokine, whereas none are detected when probes are linked with mICAM-1. Moreover, the lifetimes of these specific attachments exhibit statistical properties under stress as expected for a single diICAM-1 complex with a pair of integrin heterodimers.

Submitted July 7, 2009, and accepted for publication December 22, 2009.

*Correspondence: evanse@bu.edu or evans@phas.ubc.ca

Editor: Peter Hinterdorfer.

0006-3495/10/04/1467/9 $2.00

doi: 10.1016/j.bpj.2009.12.4316

Although much is known about integrin-mediated adhesion in biology, little is known about how cell signaling increases the physical strength and persistence of an integrin bond under force. Thus, our objective was to measure the lifetimes of ICAM-1 interactions with β_2 integrin on neutrophils under force, comparing only cells activated allosterically by millimolar concentrations of divalent cations (Mn^{2+} or Mg^{2+}) and cells stimulated by strong inside-out or outside-in signals. To test the physical properties of β_2 integrin, we used a sensitive biomembrane force probe (BFP) (12) linked covalently with a very low-density dimeric fc-chimera of ICAM-1 (diICAM-1) that formed only rare attachments to surfaces of human polymorphonuclear leukocytes or neutrophils (PMNs). The lifetimes of these bonds were measured under controlled ramps of pulling force first in 2 mM Mn^{2+} and then in 2 mM Mg^{2+} plus the chemokine IL-8 (interleukin-8) or the allosterically activating monoclonal 240Q (13,14). After we separately blocked interactions with LFA-1 by a small-molecule allosteric inhibitor specific to the α-chain (CD11a) and interactions with macrophage activation complex-1 (MAC-1) by a monoclonal antibody (mAb) specific to CD11b, we concluded that the majority (75–80%) of specific attachments between the diICAM-1 probe and PMN surfaces resulted from ICAM-1 interactions with LFA-1. Using the direct assay for off-rates demonstrated in our companion article (12), we found that the off-rates from LFA-1 under force in mM Mn^{2+} are consistent with random dissociation of an equally stressed diICAM-1 complex formed with a pair of integrin heterodimers. When we examined PMNs in 2 mM Mg^{2+} stimulated by 10 nM chemokine IL-8 (inside-out signaling), we found that the lifetimes of the dimeric attachments increased nearly 1000-fold under slow loading. Finally, we observed that similar increases in lifetime occurred when neutrophils were bound with the allosterically activating monoclonal 240Q, supporting the view that inside-out and outside-in signals occur bidirectionally along the same pathway (15).

MATERIALS AND METHODS

Soluble, five-domain monovalent ICAM-1 (mICAM-1), a recombinant human protein, was purchased from R&D Systems (Minneapolis, MN) and used without further purification. Divalent fc-chimera of human five-domain ICAM-1 (diICAM-1) was generously provided by Dr. Martyn Robinson (Celltech R&D Ltd., Berkshire, UK). Activating anti-CD18 antibody 240Q (13,14), blocking anti-CD18 antibody R15.7, and small-molecule allosteric inhibitor of LFA-1 (IC487475) (16) were obtained through an ongoing collaboration between Dr. Scott Simon and Dr. D. E. Staunton (ICOS Corp., Bothell, WA). MAC-1 blocking antibody 2LPM19fc was purchased from Dako Cytomation (Glostrop, Denmark).

Linkage to glass microspheres

To immobilize ICAM-1 or an irrelevant protein for controls on BFP tips, glass spheres (2–3 μm; Duke Scientific, Palo Alto, CA) were cleaned and functionalized with a very low concentration of the protein as described previously (see references in our companion article (12)). At the same time, a large amount of polyethylene glycol (PEG)-biotin was added to enable strong binding to the streptavidinated red cell transducer (described below). After mercapto-silane groups were bound to the microspheres, mono-and bifunctional thiol-reactive PEGs (Nektar Therapeutics, Huntsville, AL) were used to anchor the PEG-biotin and protein, respectively.

Blood cells

Fresh human blood was collected with a sterile syringe containing 10 U/mL heparin (Elkins-Sinn, Cherry Hill, NJ). Red cells were extracted by low-speed centrifugation and then linked with PEG-biotin, followed by streptavidin. To assemble the BFP (see references in our companion article (12)), a 2-μm-diameter biotinylated/protein-functionalized microsphere was attached to an avidinated red cell held by micropipet (Fig. 1 *A*). In tests of cell-surface integrin, a PMN was selected from a small microchamber sample of fresh finger-prick blood suspended in a large amount of Ca-free Hepes buffer (110 mM NaCl,10 mM KCl, 10 mM glucose, 30 mM Hepes, pH 7.35) plus 0.1% human serum albumin (Armour Pharmaceutical, Eastbourne, UK). Before experiments were conducted, each sample was washed in buffer plus EDTA/EGTA, and then mixed with HEPES buffer and a divalent salt (2 mM $MnCl_2$ or 2–5 mM $MgCl_2$). In tests of inside-out signaling, the microscope chamber sample contained buffer with 2 mM Mg^{2+} plus 10 nM of the chemokine IL-8 (R&D Systems, Minneapolis, MN). In tests of outside-in signaling, PMNs were first incubated in 2 mM of Mg^{2+} containing buffer plus 30 nM of the activating anti-CD18 monoclonal 240Q (13,14) and then placed in a microscope chamber with the same solution. See the Supporting Material for details of the method used to identify and select PMNs in the microchamber experiments.

Biomembrane force probe

When a tense BFP red cell is pressurized into a spherical shape, pulling or pushing on its microsphere tip with a small force results in an axial deflection proportional to the force (see references in our companion article (12)). Within a geometric factor of order unity, the effective spring constant, k_f, of a BFP is set by tension in the red cell membrane, which is controlled by the applied micropipet suction ΔP and scaled by the pipet radius, R_p. The BFP spring constant k_f was set to either 0.25 pN/nm or 0.5 pN/nm for the experiments reported here. The range of compressive to tensile forces accessible with a BFP is approximately -30 pN to $+300$ pN. The force precision ($\pm$1–2 pN) is set by $\pm$ 3–4 nm standard deviation (SD) error in tracking of the BFP tip displacement and the spring constant (Fig. 1 *B*). Video-image analysis provides the tracking at a sampling rate of ~1400/s. (Note: When the tip is pulled faster than 1000 nm/s, the apparent force determined from of the tip displacement must be increased by a small amount proportional to the tip velocity $\times$ 0.00048 pN-s/nm, because of viscous damping.)

Single-molecule force spectroscopy

Steady ramps of force were applied to attachments by pulling a target away after contact to the probe at constant speed V_{pull}. Although the ramps were lowered by elastic compliance of the cell interface, they remained linear in PMN tests, so the measurements of probe deflection speed V and BFP spring constant κ_f, i.e., $r_f = \kappa_f V$, determined the level of force $f = r_f t$ at any time. A piezo-driven micropipet moved PMN targets to and from contact with a BFP tip following a programmed sequence of velocities. Each touch to the BFP was limited to 0.1 s of contact and sensed by a small negative BFP deflection, as shown in Fig. 1 *B*. The PMN was then retracted at fixed speed V_{pull}. As shown in Fig. 1 *B* (*left plot*), the onset of the probe stretch often commenced a short time (Δt_o) after the zero crossing due to a small molecular length introduced by the linkage of ICAM-1 to the integrin. To determine the bond lifetime under force, the displacement at rupture X_{BFP}* was divided by the slope (velocity V) of the preceding

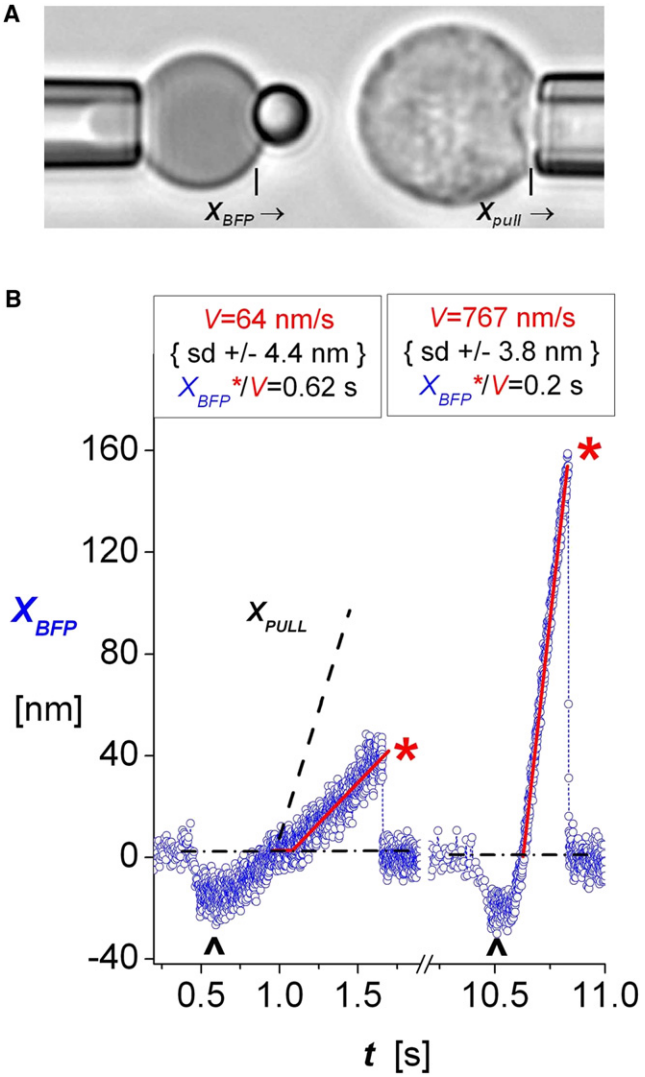

FIGURE 1 (*A*) PMN (*right*) during a course of approach and retraction to and from touch to the 2 μm glass microsphere tip of a BFP probe (*left*). The BFP tip was coated with very dilute diICAM-1 plus concentrated PEG-biotin, enabling tight adhesion to the biotinylated and avidinated red blood cell. The BFP spring constant, k_f, was set by micropipet suction control of the tension in the red cell membrane (see Materials and Methods). (*B*) Traces of BFP tip deflections X_{BFP} from tests of single diICAM-1 attachments to PMNs under slow retraction (*left*, V_{pull} = 200 nm/s) and fast retraction (*right*, V_{pull} = 2000 nm/s) both with the BFP spring constant k_f set to 0.5 pN/nm. The up marks identify 0.1 s periods of soft impingement before piezo retraction of the PMN targets, performed under feedback control. Linear regressions (*red lines*) to the measured deflections (*open blue circles*) yielded the probe deflection speeds V. The linear response to retraction defines the window of time in which the bonds experienced stress, i.e., $t = X_{BFP}*/V$. Fluctuations at intervals of 0.6 ms represent $\pm$4 nm SD in position, and given $k_f = 0.5$ pN/nm, corresponds to force fluctuations of $\pm$ 2 pN SD.

linear range, i.e., $t_i = (X_{BFP}*/V)$ as illustrated in Fig. 1 *B*. As noted previously (12,17), the ratio of cell retraction speed to probe displacement velocity, V_{pull}/V, reveals the elastic stiffness of the tip-cell interface, $\kappa_{t\sim t} = \kappa_f/(V_{pull}/V - 1)$. When PMN receptors are pulled with a spring constant of ~0.5 pN/nm, the ratios V_{pull}/V vary between 2.5 and 8 depending on the osmotic environment.

Controls for specific interactions

As a control for specific interactions with activated β_2 integrin, a diICAM-1 probe was touched to PMNs in 2 mM Mg^{2+} plus nM IL-8 in the presence of a 10 μg/mL concentration of the anti-CD18 mAb R15.7, resulting in frequencies of attachment (data not shown) indistinguishable from the nonspecifics obtained with a BSA probe (Fig. S1). To assay the relative contribution of LFA-1 to specific interactions with ICAM-1, diICAM-1 probes were touched to PMNs activated in 2 mM Mn^{2+} or in 2 mM Mg^{2+} plus nM IL-8 when exposed to 30 nM IC487475, a small-molecule inhibitor that binds to the I-domain allosteric site of CD11a. As described in Fig. S3 and overlaid as light magenta bins on histograms in Figs. 2 and 3, these controls show that 80% of diICAM-1 probe attachments to PMNs in 2 mM Mn^{2+}, and 75% of diICAM-1 attachments to PMNs in 2 mM Mg^{2+} plus nM IL-8, originated from bonds to LFA-1. This outcome was supported by the results (Fig. S4 *D*) of separate tests performed between a diICAM-1 probe and PMNs in 2 mM Mn^{2+} with MAC-1 blocked by 15 μg/mL and 6 μg/mL concentrations of the anti-CD11b mAb 2LPM19fc (Fig. S4). See the Supporting Material for further details.

Statistics of rare-point attachments

Given the low densities and limited mobility of receptors and ligands, the likelihood that attachments to receptors on PMN surfaces will form upon touch depends primarily on the area of contact and, to a much lesser extent, the contact time. Thus, by limiting the impingement force and duration of touch, one can establish uniform conditions under which attachments are formed at every touch, allowing the rare events to be characterized by Poisson statistics. Even when the contact conditions are controlled, however, procedures are needed to deal with contaminating populations that arise from nonspecific and multiple-ligand attachments.

Nonspecific attachments

We use control experiments, performed under identical probe touch and target retraction speeds, to predict the nonspecific events that are likely to occur at different levels of force. Because nonspecific interactions are limited to low forces (short times), the most reliable approach is to simply ignore the short-time statistics masked by significant numbers of nonspecifics. As shown in our companion article (12), this approach has no effect on the assay for off-rates at higher forces (longer times). Thus, overlaid as light gray bins on histograms in Figs. 2–4, we show the numbers of interactions determined by touching an irrelevant protein (bovine serum albumin) to PMNs in 2 mM Mn^{2+}. In comparison with microsphere tests (12), much higher frequencies of nonspecific interaction and range of forces arise at the surfaces of PMNs, even when performed with the same -10 pN touch and 0.1 s contact. As demonstrated in the Supporting Material, this outcome appears to stem from stronger hydrodynamic coupling (suction) when a soft cell is rapidly retracted from contact to another surface.

Procedure for treating multiple-molecule attachments

To treat multiple attachments, we use experiments to establish a stationary-random process for forming attachments, employing sensitive feedback to control contact and limiting the concentration of ligand on the probe. As such, the frequency of rare attachments A_ω provides the estimator for the likelihood of zero attachments, $P_0 = (1 - A_\omega)$, from which Poisson probabilities follow for likelihoods of a single attachment, $P_1 = (A_\omega - 1)\ln(1 - A_\omega)$, and all multiple attachments, $P_{n\geq 2} = A_\omega + (1 - A_\omega)\ln(1 - A_\omega)$. The multiple attachments are expected to share the applied force in some way and thus survive much longer than single attachments. Therefore, we use the Poisson fraction of multiple attachments, $P_{n\geq 2}/A_\omega$ ($\approx A_\omega/2 + A_\omega^2/6 + \ldots$), to truncate a small number (~10%) of raw statistics at long times and acquire arrays of putative single-attachment events $N(t_i)$. To analyze the PMN tests performed at very fast retraction speeds, we conservatively estimate this fraction by excluding the range of times that are masked by nonspecific interactions when defining the attachment frequency A_ω.

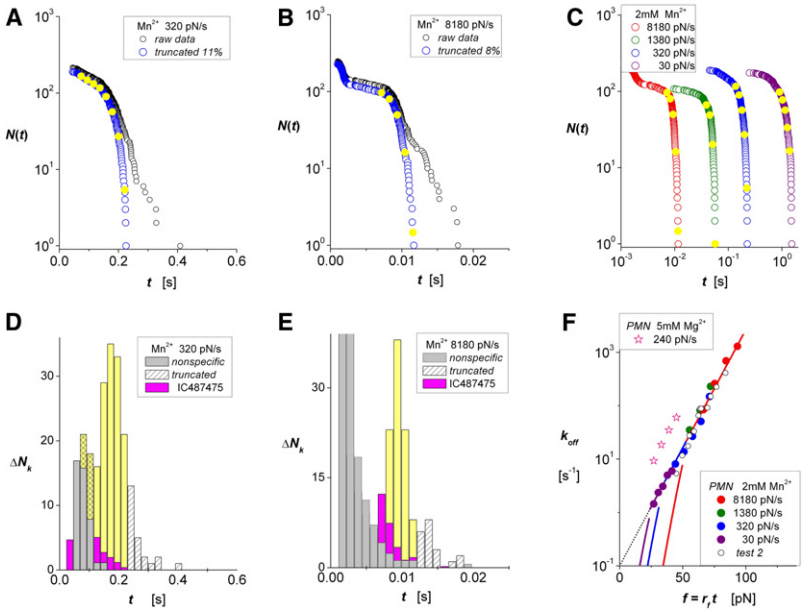

FIGURE 2 ICAM-1 interactions with LFA-1 on PMNs activated in 2 mM Mn^{2+} or 5 mM Mg^{2+}. (*A* and *B*) Lifetime data measured in 2 mM Mn^{2+} with force ramps of 320 and 8180 pN/s. Raw data (*black open circles*) appear along with arrays $N(t_i)$ (*open blue circles*) characterizing the unnormalized probability for single-attachment survival after truncating the Poisson predictions for multiple attachments. (*D* and *E*) Histograms show the unbinding transitions ΔN_k cumulated over fixed time intervals Δt in each raw data set. White-patterned bins identify the outliers truncated at long times; gray bins are nonspecifics obtained from control experiments (see Fig. S1). Intervening yellow bins show the transitions describing rates of decrease in probabilities, $(\Delta N_k/\Delta t)/N(0)$, at the bin centers t_k. Magenta bins show results obtained with LFA-1 interactions blocked by the small-molecule allosteric inhibitor IC487475. (*C*) Unnormalized probabilities $N(t_i)$ for ramps from 30 to 8180 pN/s (*open colored circles*) demonstrate the range of lifetimes obtained for all ramps in Mn^{2+}. Closed yellow circles superposed on each array identify interpolation values $N(t_k)$ found at centers t_k of the corresponding histogram bins. (*F*) The ratios $(\Delta N_k/\Delta t)/N(t_k)$ provide off-rates throughout the course of force ramps, $f_k = r_f\, t_k$, at the times defined by the bin centers in histograms (*solid colored circles*); superposed are off-rates (*open black circles*) from a second set of experiments. The linear regression (*dotted black line*) shows that the data correlate closely with a single exponential dependence on force with *e*-fold increases for each 9.6 pN beginning from a zero-force off-rate of ~0.1/s. Although limited in span, the data for activation in 5 mM Mg^{2+} parallel the data in Mn^{2+}, yet the off-rates are sevenfold faster. The pairs of colored curves describe separate regimes for off-rates that follow from the model for random dissociation of an equally stressed dimer. The threshold-like regimes (*steep-colored lines*) arise at low forces because off-rates are suppressed by the time needed for final transition from the monomer state to the unbound state. Forming a continuous exponential dependence on force for all ramps, the upper regimes (*continuous-colored lines*) show that off-rates are dominated by the initial dimer-to-monomer transition.

RESULTS AND ANALYSIS

In this work, we probed ICAM-1 interactions with β_2 integrin on PMNs to measure the kinetic rates $k_{off}(t)$ at which single-ligand attachments dissociate when subjected to pulling forces $f(t)$. As raw data for each experiment, the lifetimes t_i of attachments were measured for preset force ramps (see Materials and Methods) and arranged into an array expressing the diminishing number that survived with time, i.e., from the total number at the shortest time to one at the longest time. The raw data were then truncated by the small

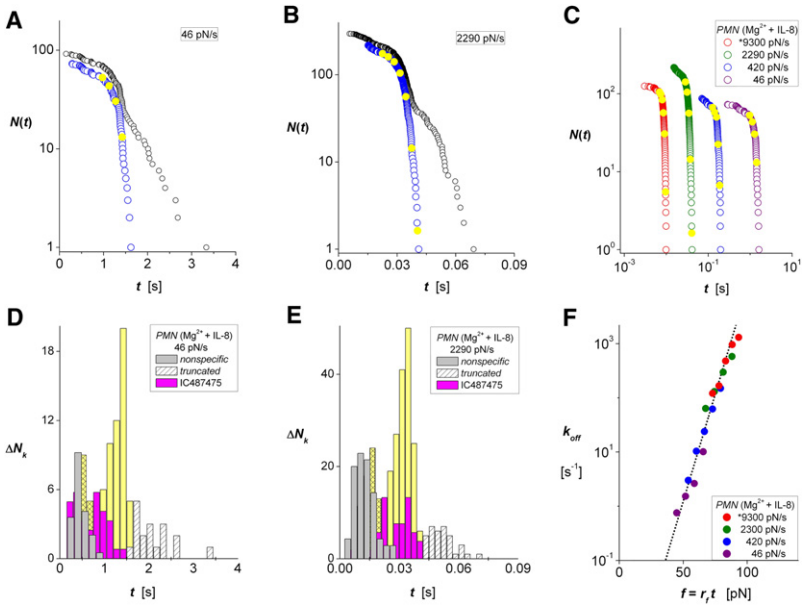

FIGURE 3 ICAM-1 interactions with LFA-1 on PMNs activated in 2 mM Mg^{2+} plus 10 nM of the chemokine IL-8. (*A* and *B*) Lifetime data measured with force ramps of 46 and 2290 pN/s, respectively. Raw data (*black open circles*) appear along with arrays $N(t_i)$ (*open blue circles*) characterizing the unnormalized probability for single-attachment survival obtained after truncating the Poisson predictions for multiple attachments. (*D* and *E*) Histograms show the unbinding transitions ΔN_k cumulated over fixed time intervals Δt in each raw data set. White-patterned bins identify the outliers truncated at long times, and gray bins are nonspecific interactions obtained from control experiments. Intervening yellow bins show the transitions describing rates of decrease in survival probabilities at the bin centers t_k. Magenta bins are results obtained with LFA-1 interactions blocked by the small-molecule allosteric inhibitor IC487475. (*C*) Unnormalized probabilities $N(t_i)$ for ramps from 46 to 9300 pN/s (*open colored circles*) demonstrate the range of lifetimes obtained for all ramps in IL-8. Closed yellow circles superposed on each array identify interpolation values $N(t_k)$ at the centers of the histogram bins. (*F*) The ratios $(\Delta N_k/\Delta t)/N(t_k)$ provide off-rates throughout the course of force ramps, $f_k = r_f\, t_k$, at the times defined by the bin centers in histograms (*solid colored circles*). The linear regression (*dotted black line*) shows that the data correlate closely with a single exponential dependence on force, with *e*-fold increases for each 5.6 pN beginning from an extremely slow zero-force off-rate of 0.0002/s.

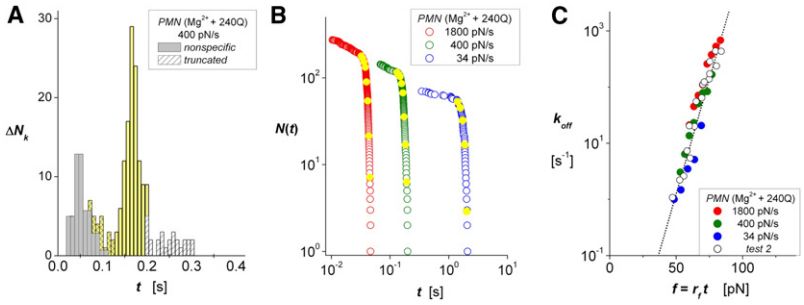

FIGURE 4 ICAM-1 interactions with β_2 integrin on PMNs in 2 mM Mg^{2+} activated allosterically by a 30 nM concentration of the antibody 240Q (13,14). (*A*) Histogram showing the unbinding transitions ΔN_k cumulated over fixed time intervals Δt for raw data obtained with a 400 pN/s ramp. White-patterned bins identify the outliers truncated at long times; gray bins are nonspecific interactions obtained from control experiments rescaled to the same number of touches. Intervening yellow bins show the transitions describing rates of decrease in survival probabilities at the bin centers t_k. (*B*) Unnormalized probabilities of survival $N(t_i)$ for three ramps from 34 to 1800 pN/s (*open colored circles*) demonstrate the range of lifetimes tested in one 240Q experiment. Closed yellow circles superposed on each array identify interpolation values $N(t_k)$ at the centers t_k of the corresponding histogram bins. (*C*) The ratios $(\Delta N_k/\Delta t)/N(t_k)$ provide off-rates throughout the course of force ramps, $f_k = r_f t_k$, at the times defined by the bin centers in histograms (*solid colored circles*). Also plotted in *C* (*open black circles*) are data for a second experiment using the ramps from 22 to 3560 pN/s. Nearly identical to data for PMN stimulation by IL-8, the linear regression (*dotted black line*) shows that the data correlate closely with a single exponential dependence on force, with *e*-fold increases for each 5.3 pN beginning from an extremely slow zero-force off-rate of 0.0001/s.

fraction of the longest times (~10%) dictated by the Poisson estimator for multiple-ligand attachments to obtain an array $N(t_i)$ of putative single-ligand attachments. Employing the two-state statistical concept described in our companion article (12), we used the arrays $N(t_i)$ and their corresponding histograms $\Delta N_k(t_k)$ of unbinding events (binned over time increments Δt) to directly assay off-rates, $k_{off}(t_k) \approx (\Delta N_k/\Delta t)/N(t_k)$, at the mean sampling times t_k in histograms. Given a deterministic history for the applied force rate $r_f(t)$, the level of force corresponding to each off-rate measurement follows simply from the integral of the force rate, $f(t_k) = \int_{o\rightarrow tk} r_f(t)\, dt$. For mICAM-1 interactions with recombinant $\alpha_L\ \beta_2$ on microspheres, we show in article I (12) that correlation of the off-rates to force is independent of whether the force is ramped over time or held constant, as demonstrated in other systems by Dudko et al. (18). However, in the PMN tests described here, the probes had to be decorated with a divalent Fc-chimera of ICAM-1 to form specific attachments. Thus, although the assay $k_{off}(t_k) \approx (\Delta N_k/\Delta t)/N(t_k)$ measures rates for dissociation of single diICAM-1 attachments, we need to consider how the transition from an initial divalent linkage to a pair of integrin heterodimers via the transient-intermediate monomer interaction with a single integrin impacts the kinetics of dissociation. As described in the Supporting Material, rates for dissociation of divalent interactions are predicted to vary throughout the course of an experiment in ways that depend on how force partitions between each arm of the divalent connection and the extent of cooperativity between the interactions. Based on these predictions and the data given below, we find that off-rates of diICAM-1 attachments to PMNs measured under ramps of force match the kinetics expected for equally stressed divalent interactions with a pair of integrin heterodimers.

ICAM-1 interactions with LFA-1 on PMNs in Mn^{2+}

In experiments involving the probing of PMNs, the large numbers of nonspecific interactions that accompany fast retraction of the PMN after it contacts the probe pose a major challenge (see Fig. S1). As reported in an earlier work (17), augmented nonspecifics result from hydrodynamic coupling (suction) between the probe tip and the soft leukocyte as the contact is rapidly separated. When we initially examined the use of slow speeds to reduce such nonspecifics, we expected to observe specific interactions when a monomeric ICAM-1 probe was touched to PMNs in Mg^{2+} or Mn^{2+}, as we found in our tests of recombinant $\alpha_L\ \beta_2$ on microspheres (12). To the contrary, however, specific attachments to PMNs could not be detected with a mICAM-1 probe, and only emerged when a diICAM-1 probe was used. At the same time, few specific attachments appeared beyond the range of nonspecifics in 2 mM Mg^{2+}, whereas numerous diICAM-1 attachments occurred when PMNs were probed in 2 mM Mn^{2+} (see Fig. S3). As noted previously (19), this behavior seems to result from the greater extension of the integrin that accompanies activation in Mn^{2+} (11). However, when we increased the concentration of Mg^{2+} to 5 mM, we obtained a reasonable population of specific ICAM-1 attachments to PMNs, although these dissociated very rapidly in comparison with those measured in 2 mM Mn^{2+} (see Fig. 2 *F*).

When we tested interactions with PMNs, we adjusted the concentration of diICAM-1 on the BFP to limit the fraction of attachments that appeared beyond the range of nonspecifics to $\leq$~20% of touches to the probe, and used the unobscured specific interactions to predict the fractions of multiple attachments. Fig. 2, *A* and *B*, show examples of the raw data for lifetimes in 2 mM Mn^{2+} (*open black circles*) obtained at slow and fast pulling speeds, along with the arrays $N(t_i)$ (*open blue circles*) for putative single-ligand events after truncation of the outliers. Histograms plotted below in Fig. 2, *D* and *E*, show the corresponding specific unbinding transitions ΔN_k (*solid yellow bins*) sandwiched between the nonspecific interactions from controls (*solid gray bins*) and the putative multiples (*white-patterned bins*). Also shown by magenta bins are results obtained in the presence of the small-molecule allosteric inhibitor IC487475, which confirmed that the majority of the ICAM-1 interactions originate from LFA-1. Even though the nonspecifics

increase significantly at fast pulling speeds, we see in Fig. 2 *E* that the fractions of specific LFA-1 bonds and outliers at the longest times are quite similar to those at the slower pulling speed in Fig. 2 *D*. Of most importance, the yellow bins in Fig. 2, *D* and *E*, identify unbinding events used as estimators for the rates of decrease in bound-state probability, $p(t_k) = -[dS/dt]_k \approx (\Delta N_k/\Delta t)/N(0)$, at the bin centers t_k. To evaluate the ratios of probability density/probability, $k_{off}(t_k) \approx (\Delta N_k/\Delta t)/N(t_k)$, we use interpolation to obtain unnormalized probabilities $N(t_k)$ at the bin center times t_k, which appear as solid yellow circles superposed on the arrays in Fig. 2, *A* and *B*. Summarizing the data for all ramp speeds, the arrays for single-attachment lifetimes are plotted on a log-log scale in Fig. 2 *C*. (Note that although the nonspecifics produce bumps in the arrays at short times (Fig. 2 *B*), the assay for off-rates is unaffected when the spurious events are confined to the beginning of an array.) As plotted in Fig. 2 *F* versus forces at the bin center times ($f_k = r_f\, t_k$), the logarithms of the off-rates for diICAM-1 attachments to LFA-1 on PMNs in 2 mM Mn^{2+} at each ramp speed (*solid colored circles*) increase exponentially with the pulling force. Extrapolating to a zero-force rate $\approx$ 0.1/s, the linear regression in Fig. 2 *F* shows that the off-rates increase *e*-fold for each $f_\beta \approx 9.6$ pN increment in force under ramps from 30 to 8000 pN/s. (Data from a single ramp test in 5 mM Mg^{2+} (*open pink stars*) also appear in Fig. 2 *F* paralleling the measurements in Mn^{2+} but at much faster off-rates.) Viewed simply, the data in Fig. 2 *F* seem to match the model proposed by Bell (20) many years ago, in which a critical distance $x_\beta = k_BT/f_\beta$ defines the force needed to lower the activation energy barrier governing off-rate by one thermal energy unit k_BT [$\approx 4.08 \times 10^{-21}$ J] for room-temperature (23°C) experiments. However, as described next, this outcome is unusual given that the single attachments are likely to be dimeric.

Off-rates of dimeric bonds under force

The Poisson analysis used to estimate multiples characterizes random sites of attachment in a fixed area of contact. If it is sufficiently dilute, the fraction of multiple-site attachments will be little affected by the valence of the ligand. Thus, lacking information other than the attachment frequency, we cannot distinguish single diICAM-1 attachments that involve dimeric interactions with an adjacent pair of integrin heterodimers from interactions involving a single heterodimer. Yet, the requirement for diICAM-1, and evidence from FRET experiments (11) strongly imply that the majority of attachments in Mn^{2+} arise from divalent connections to a clustered pair of heterodimers. Even though off-rates of mICAM-1 from $\alpha_L\,\beta_2$ on microspheres in Mn^{2+} follow a single exponential dependence on force (12), there is no reason to expect the same outcome for diICAM-1 attachments to a pair of LFA-1 on PMNs. Along with the dissociation kinetics of the monomeric interaction, the determining factors for dimer off-rates include the manner in which the pulling force partitions between the two interactions, and the extent of cooperativity in their dissociation. As shown by the limiting cases in the Supporting Material, the only trivial outcome is when the two monomeric interactions dissociate cooperatively (i.e., at the same instant in time, behaving as a one bond). When the two monomeric interactions dissociate randomly without rebinding, dissociation involves a three-state process beginning with the transition at a rate $k_{2\to1}(t)$ from the dimer state [probability $S_2(t)$], proceeding through a transient monomeric state [probability $S_1(t)$], and finally unbinding at a rate $k_{1\to0}(t)$. Thus, the dimer off-rates depend explicitly on the transient occupancies of dimer and monomer states, $k_{off}(t) = k_{1\to0}(t)\ [S_1(t)/S_2(t)]\ /\ [S_1(t)/S_2(t) + 1]$.

By idealizing transition rates for the uncooperative monomer interactions as exponential functions of force, we can easily see how dimer off-rates depend on the limiting conditions of force partitioning (see Supporting Material). At one limit, labeled the ''zipper dimer'', the force f acts initially on one interaction until it dissociates, transferring the force to the remaining interaction until failure occurs. Thus, each transition is described by the force-dependent rate, $k_{1\to0} = k_o \exp(f/f_\beta)$. Stressed with a force ramp [$f(t) = r_f\, t$], the dimer off-rate becomes

$$k_{Zdimer}(f) = k_o \exp(f/f_\beta)\left[\exp(f/f_\beta) - 1\right] / \left[c_r + \exp(f/f_\beta) - 1\right] \quad (1)$$

which shifts with the dimensionless ramp speed $c_r \equiv r_f/(k_o f_\beta)$ and curves sharply downward toward zero at low forces on a logarithmic scale (Fig. S8 *A*). At high forces, the dimer off-rate approaches the limiting rate for monomer dissociation.

At the other limit, labeled the ''parallel-loaded dimer'', the force is initially split between the two interactions ($f/2$ each) until one dissociates, and then the full force f passes to the remaining interaction. The first transition is described by a rate $k_{2\to1} = 2\, k_o \exp(f/2f_\beta)$, and the second is described by $k_{1\to0} = k_o \exp(f/f_\beta)$. In contrast to a zipper dimer, the off-rates for equally stressed dimers are characterized by two regimes (Fig. S8 *B*) of behavior above/below a crossover force that again depends on the dimensionless ramp speed, $f_\otimes = 2 f_\beta \ln(2 + c_r^{1/2})$. At low forces, $f < f_\otimes$, the time needed for transition from the monomer state to the unbound state significantly retards dissociation, and off-rates follow the approximation:

$$k_{PLdimer}(f) \approx k_o \exp(f/f_\beta)\left[\exp(f/2f_\beta) - 1\right] / \left[\exp(f/2f_\beta) - 1 + c_r/2\right] \quad (2)$$

At high forces, $f > f_\otimes$, off-rates are dominated by the initial dimer-to-monomer transition and thus follow the exponential:

$$k_{PLdimer}(f) \approx 2k_o \exp(f/2f_\beta) \quad (3)$$

Hence, off-rates for equally stressed dimers exhibit a threshold-like response (Fig. S8 *B*), and dissociate frequently only when forces exceed $f_\otimes = 2\, f_\beta \ln(2 + c_r^{1/2})$.

Comparing these models with the results for diICAM-1 interactions with PMNs in Mn^{2+}, we find that only the equally stressed dimer model can correlate with the off-rate behavior. The pairs of colored curves for each force ramp in Fig. 2 *F* identify the two off-rate regimes approximated by Eqs. 2 and 3. The low-force regimes (Eq. 2) lie just below the onset of measured values. On the other hand, the high-force regimes form a continuous line that correlates well with all of the measurements.

ICAM-1 interactions with LFA-1 on PMNs after IL-8 stimulation

To test the impact of inside-out signaling, we probed PMNs within 5–10 min after exposure to saturating (10 nM) concentrations of the chemokine IL-8 in 2 mM Mg^{2+}. Consistent with previous studies (21), the fraction of specific diICAM-1 attachments to PMNs decreased monotonically with the time after exposure to IL-8, essentially vanishing by ~30 min (data not shown). Even so, the specific ICAM-1 interactions appeared at the same position in lifetime histograms. When we collected data only within the first 5–10 min, we had to repeat the PMN tests in IL-8 several times to acquire adequate statistics. The examples in Fig. 3, *A* and *B*, show the raw data for lifetimes (*open black circles*) obtained at slow and intermediate pulling speeds accompanied by the arrays $N(t_i)$ (*open blue circles*) of single-ligand events after truncation of the putative outliers. Histograms plotted below in Fig. 3, *D* and *E*, show the corresponding unbinding transitions ΔN_k (*solid yellow bins*) sandwiched between the distributions of nonspecifics (*solid gray bins*) and the truncated fractions of multiples (*white-patterned bins*). The magenta bins are results obtained in the presence of the small-molecule allosteric inhibitor IC487475, which confirmed that the majority of specific ICAM-1 attachments to PMNs stimulated by IL-8 in Mg^{2+} originate from LFA-1. Summarizing all ramp speeds, we show the arrays of putative single-attachment lifetimes plotted on a log-log scale in Fig. 3 *C* along with the interpolated values corresponding to the bin center times t_k in histograms. Finally, the estimators for probability density/probability are plotted on a logarithmic scale in Fig. 3 *F* versus the forces at the bin center times ($f_k = r_f t_k$). A double slow/hyperfast ramp sequence (identified by an asterisk before the 9300 pN/s ramp in Fig. 3, *C* and *F*; cf. Fig. S5 *A*) was used to extend the force range while minimizing the effect of hydrodynamic coupling (see details in the Supporting Material). Including the data obtained at all ramp speeds, it can be seen that the off-rates for diICAM-1 interactions with PMNs stimulated by IL-8 in 2 mM Mg^{2+} increased exponentially with pulling forces, as when activated in Mn^{2+}. Yet, the linear regression in Fig. 3 *F* reveals that inside-out signaling in PMNs increased the apparent unstressed lifetime $1/k_o$ of the LFA-1 interactions by 500-fold, i.e., $k_o \approx 0.0002$/s, and significantly decreased the thermal force scale for exponentiation, i.e., $f_\beta \approx 5.6$ pN.

ICAM-1 interactions with β_2 integrin on PMNs activated allosterically by mAb 240Q

Finally, to test the impact of increased outside-in signaling, we probed diICAM-1 interactions with the high-affinity state of β_2 integrin induced on PMNs by the activating anti-CD18 antibody 240Q (13,14) in 2 mM Mg^{2+}. The experiments were performed at several ramp rates ranging from 20 pN/s to 3600 pN/s, and yielded distributions with narrow peaks of specific interactions as shown by the example in Fig. 4 *A* (see Fig. S6 *A* for a repeat experiment). Similarly to the distributions for chemokine stimulation shown in Fig. 3, *D* and *E*, narrow peaks of unbinding transitions in the histograms indicate precipitous shortening of bond lifetimes under the rising force, which is clearly evident in the arrays $N(t_i)$ (*open blue circles*) plotted for one experiment in Fig. 4 *B* (see the other set in Fig. S6 *B*). Using the statistics of bond survival and histograms obtained from both 240Q tests, we determined the off-rates at the bin center times t_k. The data are plotted in Fig. 4 *C* versus the forces ($f_k = r_f t_k$) for each ramp speed along with the cumulated results from the second experiment (Fig. S6 *C*). As was the case for inside-out signaling, outside-in signaling through 240Q increased the apparent unstressed lifetime $1/k_o$ of the diICAM-1 interactions by 1000-fold, i.e., $k_o \approx 0.0001$/s, and significantly decreased the thermal force scale for exponentiation, i.e., $f_\beta \approx 5.3$ pN.

CONCLUSIONS

By probing diICAM-1 interactions with β_2 integrin on PMNs in this study, we were able to quantify the rates of bond dissociation at each level of force throughout the course of constant-speed pulling experiments. As demonstrated in our companion article (12) for mICAM-1 interactions with recombinant α_L β_2 on microspheres, the direct assay for off-rates is based solely on statistics of bond lifetimes; correlations to force follow independently from the probe history of force versus time. With precision control of experiments, the Poisson estimates for rare multiple attachments provide an effective means to extract a very high proportion of single-molecule attachments. We acquired these statistics with force ramps from 10 to 10000 pN/s, and determined the rates for dissociation of single diICAM-1 molecules under force from PMNs over a wide range of activating buffer conditions from Mn^{2+} or Mg^{2+} alone to Mg^{2+} plus saturating concentrations of the chemokine IL-8 or the activating monoclonal 240Q. The results for PMNs in the presence and absence of the LFA-1 inhibitor IC487475 (Fig. S3) led us to conclude that the off-rates measured in the absence of inhibitor are dominated by kinetics of interactions between diICAM-1 and LFA-1. This conclusion was further confirmed by tests with MAC-1 blocked on PMNs by the mAb 2LPM19fc (Fig. S4). Analysis of the few remaining attachments to PMNs in Mn^{2+} plus IC47475 indicates that

the diICAM-1 interactions with MAC-1 dissociate much faster and are mechanically weaker than the interactions with LFA-1 (Fig. S3 *F*).

Beyond the range of low forces masked by nonspecifics, the off-rates for diICAM-1 bonds to LFA-1 in all cases followed single exponential dependences on pulling force, extending progressively upward with increases in ramp speed. Given the requirement for diICAM-1 in our tests and the evidence from FRET studies (11), we considered the results for off-rates under force ramps in terms of dimer dissociation, and sought a model for internal dynamics that would be consistent with the observed exponential dependence on force. Assuming a monomer dissociation rate that depends exponentially on force, the simplest model for the dimer dissociation process begins with equally stressed monomer bonds to a pair of integrin heterodimers. These interactions then dissociate either separately in random sequence or cooperatively as a single bond. In the absence of cooperativity, off-rates are dominated by the initial dimer-to-monomer transition, which is characterized by twice the force-free off-rate ($2k_o$) and twice the thermal force scale ($2f_\beta$) of a single monomer interaction. Consistent with the apparent threshold-like dependence on loading speed expected for random dimeric dissociation, the dependence of unbinding rate on force, $k_{off} \approx 0.1/s \exp(f/9.6pN)$, when activated allosterically by Mn^{2+} implies that each monomer interaction unbinds at a rate described by $k_{1\to0} \approx 0.05/s \exp(f/4.8pN)$. By comparison, the dramatic reduction in the zero-force off-rate (k_o ~0.0001/s), and the ~2-fold smaller thermal force scale (f_β ~5.3–5.6 pN) when PMNs in Mg^{2+} were stimulated by IL-8 or 240Q suggest that strong inside-out or outside-in signaling can induce a cooperative dimeric state in which the two monomer interactions unbind simultaneously under force.

Of interest, the prolongation of lifetimes from levels found in probing diICAM-1 attachments to PMNs in 5 mM Mg^{2+} to the levels obtained in Mg^{2+} plus IL-8 or the activating monoclonal 240Q match the range of ICAM-1 off-rates measured for intermediate affinity to hyperaffinity mutants of the αI domain of LFA-1 in previous surface plasmon resonance experiments by Jin et al. (22). Since none of the mutations mapped to the ICAM-1 binding interface, they concluded that the major increase in lifetimes reflected an allosteric shape-shifting pathway, whereby the metal ion-dependent adhesion site switched from a closed to an open conformation (22). The identical impact of IL-8 and the activating monoclonal 240Q on off-rates of diICAM-1 attachments to LFA-1 on PMNs (Fig. 4 *C*) provides strong evidence that a similar conformational switching accompanies the inside-out and outside-in signaling processes in PMNs, as concluded previously (15). A good model for the putative cooperative divalent arrangement is the asymmetric crystallographic unit formed by domains 1–2 of parallel ICAM-1 molecules and the two αI domains of LFA-1 that appear in Fig. 1 *C* of Shimaoka et al. (23).

SUPPORTING MATERIAL

Eight figures are available at http://www.biophysj.org/biophysj/supplemental/S0006-3495(10)00083-4.

This work was supported by National Institutes of Health grants HL65333, HL31579 (to E.E.), and AI47294 (to S.I.S.).

REFERENCES

1. McEver, R. P. 2001. Adhesive interactions of leukocytes, platelets, and the vessel wall during hemostasis and inflammation. *Thromb. Haemost.* 86:746–756.
2. Hynes, R. O. 2002. Integrins: bidirectional, allosteric signaling machines. *Cell.* 110:673–687.
3. Shimaoka, M., J. Takagi, and T. A. Springer. 2002. Conformational regulation of integrin structure and function. *Annu. Rev. Biophys. Biomol. Struct.* 31:485–516.
4. Arnaout, M. A., B. Mahalingam, and J. P. Xiong. 2005. Integrin structure, allostery, and bidirectional signaling. *Annu. Rev. Cell Dev. Biol.* 21:381–410.
5. Luo, B. H., and T. A. Springer. 2006. Integrin structures and conformational signaling. *Curr. Opin. Cell Biol.* 18:579–586.
6. Nishida, N., C. Xie, …, T. A. Springer. 2006. Activation of leukocyte β_2 integrins by conversion from bent to extended conformations. *Immunity.* 25:583–594.
7. Carman, C. V., and T. A. Springer. 2003. Integrin avidity regulation: are changes in affinity and conformation underemphasized? *Curr. Opin. Cell Biol.* 15:547–556.
8. Geiger, B., A. Bershadsky, …, K. M. Yamada. 2001. Transmembrane extracellular matrix-cytoskeleton cross talk. *Nat. Rev. Mol. Cell Biol.* 2:793–805.
9. Dustin, M. L., and D. R. Colman. 2002. Neural and immunological synaptic relations. *Science.* 298:785–789.
10. Lee, K.-H., A. R. Dinner, …, A. S. Shaw. 2003. The immunological synapse balances T cell receptor signaling and degradation. *Science.* 302:1218–1222.
11. Kim, M., C. V. Carman, …, T. A. Springer. 2004. The primacy of affinity over clustering in regulation of adhesiveness of the integrin $\alpha_L\beta_2$. *J. Cell Biol.* 167:1241–1253.
12. Evans, E., K. Kinoshita, …, A. Leung. 2010. Long-lived, high-strength states of ICAM-1 bonds to β_2 integrin: I. Lifetimes of bonds to recombinant α_L β_2 under force. *Biophys. J.* 98:1458–1466.
13. Lupher, Jr., M. L., E. A. Harris, …, D. E. Staunton. 2001. Cellular activation of leukocyte function-associated antigen-1 and its affinity are regulated at the I domain allosteric site. *J. Immunol.* 167:1431–1439.
14. Beals, C. R., A. C. Edwards, …, D. E. Staunton. 2001. CD18 activation epitopes induced by leukocyte activation. *J. Immunol.* 167:6113–6122.
15. Luo, B. H., C. V. Carman, and T. A. Springer. 2007. Structural basis of integrin regulation and signaling. *Annu. Rev. Immunol.* 25:619–647.
16. Green, C. E., U. Y. Schaff, …, S. I. Simon. 2006. Dynamic shifts in LFA-1 affinity regulate neutrophil rolling, arrest, and transmigration on inflamed endothelium. *Blood.* 107:2101–2111.
17. Evans, E., V. Heinrich, …, K. Kinoshita. 2005. Nano- to microscale dynamics of P-selectin detachment from leukocyte interfaces. I. Membrane separation from the cytoskeleton. *Biophys. J.* 88:2288–2298.
18. Dudko, O. K., G. Hummer, and A. Szabo. 2008. Theory, analysis, and interpretation of single-molecule force spectroscopy experiments. *Proc. Natl. Acad. Sci. USA.* 105:15755–15760.
19. Dransfield, I., C. Cabañas, …, N. Hogg. 1992. Divalent cation regulation of the function of the leukocyte integrin LFA-1. *J. Cell Biol.* 116:219–226.

20. Bell, G. I. 1978. Models for the specific adhesion of cells to cells. *Science*. 200:618–627.

21. Lum, A. F. H., C. E. Green, …, S. I. Simon. 2002. Dynamic regulation of LFA-1 activation and neutrophil arrest on intercellular adhesion molecule 1 (ICAM-1) in shear flow. *J. Biol. Chem.* 277: 20660–20670.

22. Jin, M., G. Song, …, T. A. Springer. 2006. Directed evolution to probe protein allostery and integrin I domains of 200,000-fold higher affinity. *Proc. Natl. Acad. Sci. USA.* 103:5758–5763.

23. Shimaoka, M., T. Xiao, …, T. A. Springer. 2003. Structures of the α L I domain and its complex with ICAM-1 reveal a shape-shifting pathway for integrin regulation. *Cell.* 112:99–111.